Available online at www.sciencedirect.com
SCIENCE DIRECT®
Journal of Magnetic Resonance 170 (2004) 244–251
JMR Journal of Magnetic Resonance
www.elsevier.com/locate/jmr

Optimized pathway selection in intraresidual triple-resonance experiments

Helena Tossavainen, Perttu Permi*

NMR Laboratory, Structural Biology and Biophysics Program, Institute of Biotechnology, P.O. Box 65, FIN-00014, University of Helsinki, Helsinki, Finland

Received 16 April 2004; revised 14 June 2004
Available online 28 July 2004

Abstract

An optimized intraresidual pulse sequence element with better sensitivity and suppression of sequential cross peaks is presented. Concatenation of three magnetization transfer delays allows their independent setting, in accordance with the relaxation properties of the individual spins, without concomitantly prolonging the pulse sequence. Additionally, implementations of the scheme to HNCA, HNCACB, and the TROSY based triple-resonance experiments are proposed. The feasibility of the new element was verified by recording HNCA and HNCACB on the small 8.6 kDa protein ubiquitin. The corresponding HNCA–TROSY experiment was tested on a larger protein, the 30.4 kDa Cel6A from the thermophilic soil bacterium *Thermobifida fusca* at 800 ^{1}H MHz.

Keywords: Assignment; Cel6A; HNCA; HNCACB; TROSY; Ubiquitin

1. Introduction

Sequence-specific resonance assignment is the first step in detailed structural studies of proteins. Typically, signals are assigned to their sources in the chemical structure by recording a pair of complementary experiments, e.g., HNCA/HN(CO)CA [1,2], which yield intraresidual $^{1}H^{N}(i)$, $^{15}N(i)$, and $^{13}C^{\alpha}(i)$, and sequential $^{1}H^{N}(i)$, $^{15}N(i)$, and $^{13}C^{\alpha}(i-1)$ correlations [3–5]. The assignment process can be made easier by extending the HNCA/HN(CO)CA pair to cover also $^{13}C^{\beta}$ spins in the HNCACB/HN(CO)CACB experiments [6–10]. The $^{13}C^{\beta}$ spins provide precious information on residue type, and the $^{13}C^{\beta}$ chemical shifts are also indicative of the secondary structure of protein [11]. In principle, the sequential assignment can then be established using only the HNCA (or HNCACB) experiment. However, in practice, a complementary experiment like the HN(CO)-CA is needed to verify the assignments as intraresidual and interresidual cross peaks cannot always be distinguished from each other based on their intensity difference in the HNCA spectrum.

Recently, a novel coherence transfer scheme leading to solely intraresidual cross peak was introduced [12–15]. The intraresidual HNCA (iHNCA) experiment, as well as its extended applications, e.g., intra-HNCACB or intra-HN(CA)HA, display only intraresidual $^{1}H^{N}(i)$, $^{15}N(i)$, and $X(i)$ ($X = {}^{13}C^{\alpha}$, $^{13}C^{\beta}$, or $^{1}H^{\alpha}$) connectivities [16]. Depending on the selected coherence transfer route, the iHNCA experiment can be applied to both smaller and larger proteins [12]. In this paper we show that the intraresidual transfer can be optimized further for both improved sensitivity especially on α-helical regions and enhanced suppression of the undesired coherence transfer pathway leading to the undesired sequential cross peaks.

* Corresponding author. Fax: +358-9-191-595-41.
E-mail address: perttu.permi@helsinki.fi (P. Permi).

1090-7807/$ - see front matter © 2004 Elsevier Inc. All rights reserved.
doi:10.1016/j.jmr.2004.06.018

2. Theory

Fig. 1A illustrates the streamlined intraresidual pulse sequence element. The optimized sequence combines the best features of two experiments, iHNCA [12] and intra-HNCA [15] and hence improves the overall sensitivity and suppression of undesired sequential cross peaks. The details of both experiments can be found in the original papers and here, we emphasize only the differing parts regarding the proposed experiment.

Let us first consider the key element of all intraresidual experiments, i.e., the coherence transfer step that selects the desired intraresidual pathway. Fig. 1B shows the transfer step used in the iHNCA scheme [12,14]. The ^{15}N magnetization is initially converted into the triple antiphase form with respect to $^{13}C^{\alpha}(i)$, $^{13}C^{\alpha}(i-1)$, and $^{13}C'(i-1)$ spins by utilizing concatenated delays $4T_a$ and $2T_N$. Subsequently, the magnetization is converted into the $^{13}C'(i-1)$ coherence followed by the $^{13}C'$–$^{13}C^{\alpha}$ INEPT step ($2T_C$) during which the one-bond coupling between the $^{13}C'(i-1)$ and $^{13}C^{\alpha}(i-1)$ spins is refocused. This enables the labeling of the $^{13}C^{\alpha}(i)$ chemical shift alone, to a first order, during the succeeding t_1 period which follows the last 90°($^{13}C^{\alpha}$) pulse with phase ϕ_2.

The intraresidual pathway selection proposed by Brutscher [15] is depicted in Fig. 1C. The ^{15}N single-quantum coherence evolves with active couplings to the neighboring $^{13}C^{\alpha}(i)$, $^{13}C^{\alpha}(i-1)$, and $^{13}C'(i-1)$ spins during the delay $2T_N$, and is converted into the ^{15}N–$^{13}C'$ multiple-quantum coherence at time point a. During the ensuing $^{13}C'$–$^{13}C^{\alpha}$ INEPT step ($2T_C$), the coupling evolution between the ^{15}N and $^{13}C^{\alpha}(i)$, and $^{13}C^{\alpha}(i-1)$ spins continues, whereas the one-bond coupling between the $^{13}C'(i-1)$ and $^{13}C^{\alpha}(i-1)$ nuclei is simultaneously refocused. Hence, as in the element in Fig. 1B, the desired coherence is antiphase with respect to only $^{13}C^{\alpha}(i)$ spin prior to the conversion into the $^{13}C^{\alpha}(i)$ transverse magnetization for the chemical shift labeling.

The corresponding transfer function for the intraresidual element in Fig. 1B is given with Eq. (1):

$$\sin(2\pi^1 J_{NC'}T_N)\sin(4\pi^1 J_{NC^{\alpha}}T_a)\sin(4\pi^2 J_{NC^{\alpha}}T_a) \times \sin(2\pi^1 J_{C'C^{\alpha}}T_C)\exp(-4T_a/T_{2,N}) \times \exp(-2T_C/T_{2,C'}). \quad (1)$$

Nominal delays for $2T_N$, $2T_C$, and $4T_a$ are 33.3, 9.1, and ~43–52 ms, respectively. The $T_{2,N}$ and $T_{2,C'}$ are transverse relaxation times for the ^{15}N and $^{13}C'$ coherences, respectively. The $^1J_{NC'}$ and $^1J_{C'C^{\alpha}}$ scalar couplings are usually between 14–16 and 51–55 Hz, respectively. Instead, the one-bond $^1J_{NC^{\alpha}}$ coupling has a weak correlation, and the two-bond $^2J_{NC^{\alpha}}$ coupling has a strong one with the protein's backbone conformation [17,18]. The $^1J_{NC^{\alpha}}$ typically varies between 7 and 13 Hz, whereas $^2J_{NC^{\alpha}}$ normally varies between 5 and 9 Hz. The average values for the $^1J_{NC^{\alpha}}$ and $^2J_{NC^{\alpha}}$ scalar couplings found in α-helices are 9.6–9.9 and 6.3–6.4 Hz, respectively. The average coupling constants for residues in β-strands are larger, i.e., 10.9–11.2 and 8.3–8.4 Hz, respectively [17,18]. For this reason, the maximum amplitude for the $^1J_{NC^{\alpha}} + {}^2J_{NC^{\alpha}}$ transfer is higher for residues in β-strands. On the other hand, the transfer maximum for α-helical residues is reached when the transfer delay is close to 52 ms. In addition, the overall suppression of the sequential pathway is optimal at $4T_a \sim 50$ ms [12].

Analogously, the transfer function for the intra-HNCA element [15] can be described using Eq. (2)

$$\sin(2\pi^1 J_{NC'}T_N)\sin(2\pi^1 J_{NC^{\alpha}}(T_N+T_C)) \times \sin(2\pi^2 J_{NC^{\alpha}}(T_N+T_C))\sin(2\pi^1 J_{C'C^{\alpha}}T_C) \times \exp(-2T_N/T_{2,N})\exp(-2T_C/T_{2,MQ}), \quad (2)$$

where $T_{2,MQ}$ is the transverse relaxation time for the ^{15}N–$^{13}C'$ multiple-quantum coherence. It can be appreciated that in the scheme in Fig. 1B, the delays can be adjusted independently from each other, i.e., if the transverse relaxation time of ^{15}N spin is sufficiently long, the delay $4T_a$ can be set to approximately 50–52 ms, which is optimal for residues in α-helix [12]. This value provides also the best overall suppression of the sequential pathway [12]. In addition, at the highest magnetic field strength where the spin relaxation of the $^{13}C'$ nucleus can be very fast owing to its large chemical shift anisotropy (CSA) [5,19–21], the delay $2T_C$ can be shortened while still maintaining an optimal ^{15}N–$^{13}C^{\alpha}$ transfer time on the slowly relaxing ^{15}N TROSY multiplet. In contrast, the pulse sequence element in Fig. 1C does not allow independent setting of individual transfer delays. The delay $2T_N$ is set to 34 ms, whereas the delay $2T_C$ is set to 9 ms [15]. The transfer delay for the creation of double antiphase coherence with respect to $^{13}C^{\alpha}(i)$/$(i-1)$ spins then becomes 43 ms. This value is close to optimal for residues in β-strands but clearly less than optimal for residues in α-helices [12]. It is noteworthy that the transfer for residues in helical substructures is the limiting factor in the intraresidual experiments. Furthermore, if the delay $2T_C$ is shortened to alleviate the sensitivity loss due to the rapid $^{13}C'$ spin relaxation, the ^{15}N–$^{13}C^{\alpha}$ transfer is also compromised. Likewise, when the $2T_N$ is altered, it affects both the $\sin(2\pi^1 J_{NC'}T_N)$ and $\sin(2\pi^1 J_{NC^{\alpha}}(T_N+T_C))$ $\sin(2\pi^2 J_{NC^{\alpha}}(T_N+T_C))$ terms owing to their dependence on $2T_N$. On the contrary, the overall length of the element in Fig. 1C is significantly shorter than the element in Fig. 1B, which counterbalances their performance.

Now, let us focus on the optimized pulse sequence element in Fig. 1A. In this scheme, all the three delays, $4T_a$, $2T_N$, and $2T_C$ are concatenated. The delays can be altered independently (within reasonable values)

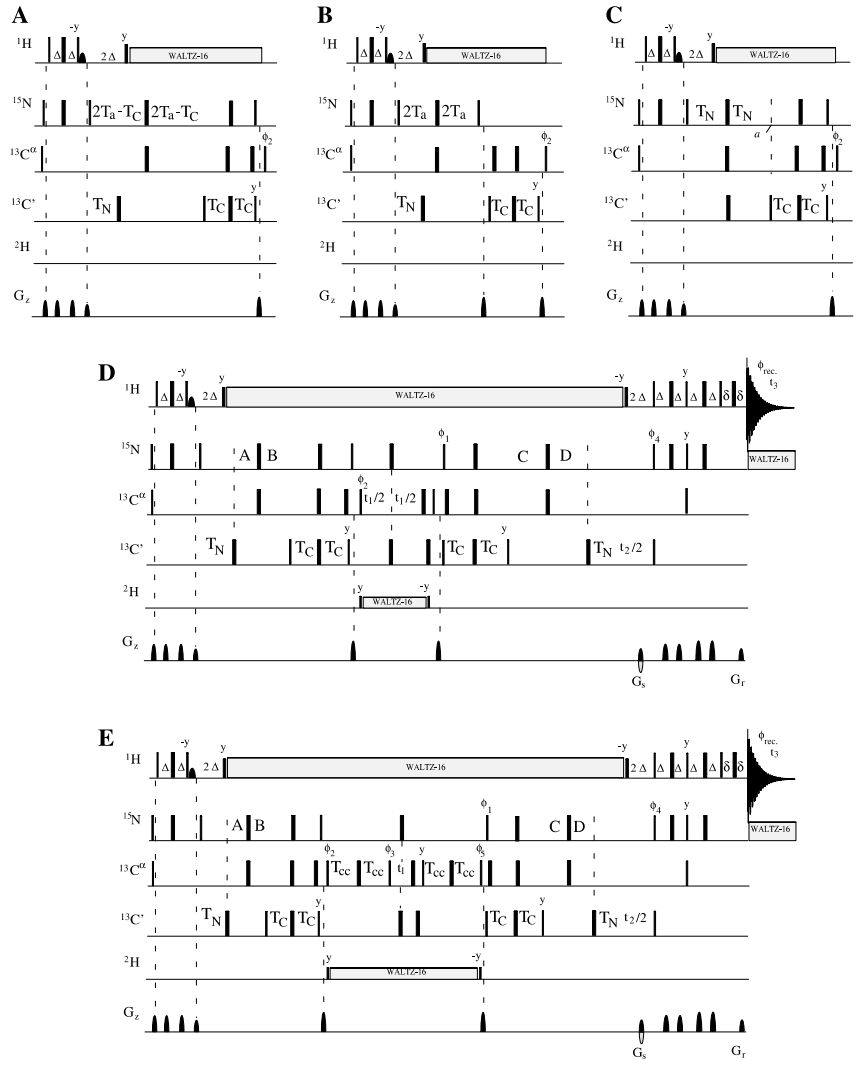

Fig. 1. The intraresidual transfer elements for the selection of solely intraresidual coherence transfer pathway. (A) The streamlined intraresidual pulse sequence element, (B) the iHNCA element [12], (C) the intra-HNCA scheme [15]. (D) The new *out and back* type intraresidual HNCA (iHNCA) and (E) HNCACB (iHNCACB) experiments for recording only intraresidual $^{13}C^{\alpha}(i)$, $^{15}N(i)$, and $^{1}H^{N}(i)$ and $^{13}C^{\alpha}(i)/^{13}C^{\beta}(i)$, $^{15}N(i)$, and $^{1}H^{N}(i)$ connectivities in $^{13}C/^{15}N/^{2}H$ labeled proteins. Narrow and wide bars correspond to 90° and 180° flip angles, respectively, applied with phase x unless otherwise indicated. Half-ellipse denotes water selective 90° pulse to obtain water flip-back [27]. All 90° (180°) pulses for $^{13}C'$, $^{13}C^{\alpha}$, and $^{13}C^{\alpha}/^{13}C^{\beta}$ are applied with a strength of $\Omega/\sqrt{15}$ ($\Omega/\sqrt{3}$), where Ω is the frequency difference between the centers of the $^{13}C'$, $^{13}C^{\alpha}$, and $^{13}C^{\alpha}/^{13}C^{\beta}$ regions. The ^{1}H, ^{15}N, $^{13}C'$, $^{13}C^{\alpha}$, and $^{13}C^{\alpha}/^{13}C^{\beta}$ carrier positions are 4.7 (water), 120 (center of ^{15}N spectral region), 175 (center of $^{13}C'$ spectral region), 57 ppm (center of $^{13}C^{\alpha}$ spectral region), and 46 ppm (center of $^{13}C^{\alpha}/^{13}C^{\beta}$ region), respectively. All $^{13}C'$ and $^{13}C^{\alpha}$ off-resonance pulses are applied with phase modulation by Ω. In the iHNCA scheme (D), the ^{13}C transmitter is initially set to the $^{13}C'$ region, shifted to 57 ppm just before the 90° ϕ_2 pulse, and shifted back to 175 ppm after the 90° ($^{13}C^{\alpha}$) pulse following the t_1 period. In the iHNCACB scheme (E), the ^{13}C carrier is set to the $^{13}C'$ region, shifted to 46 ppm just before the pulse with phase ϕ_2, and shifted back to 175 ppm after the 90° ($^{13}C^{\alpha}/^{13}C^{\beta}$) pulse (phase y) succeeding the second $2T_{CC}$ period. Optional deuterium decoupling can be applied during the $2T_{CC}$ and t_1 periods in (per)deuterated samples. Quadrature detection and coherence pathway selection in the ^{15}N dimension is obtained using the sensitivity-enhanced gradient selection [28,29]. The echo and anti-echo signals are collected separately by inverting the sign of the G_s gradient pulse together with the inversion of ϕ_4. In addition to echo/anti-echo selection, ϕ_1 and ϕ_{rec} are incremented according to States–TPPI protocol [30].Quadrature detection in the $^{13}C^{\alpha}/(^{13}C^{\beta})$ dimension is obtained by applying States–TPPI to ϕ_2 (scheme D), and to ϕ_2 and ϕ_3 (scheme E). Pulsed field gradients are inserted as indicated for coherence transfer pathway selection and residual water suppression. The nominal delay durations are: $\Delta = 1/(4J_{HN})$; $T_N = 1/(4J_{NC'})$; $2T_a \sim 25$ ms; $T_C = 1/(4J_{C'C^{\alpha}})$; $T_{CC} = 1/(6\text{–}8J_{C^{\alpha}C^{\beta}})$; A = D = $2T_a - (T_N + T_C)$; B = $2T_a - T_C$; C = $2T_a - (T_C + t_2/2)$; δ = gradient + field recovery delay. Gradient strengths (durations): $G_s = 30$ G/cm (1.25 ms), $G_r = 29.6$ G/cm (0.125 ms). The WALTZ-16 sequence [31] was used to decouple ^{1}H during heteronuclear coherence transfer and ^{15}N during acquisition. Phase cycling: $\phi_1 = x$; $\phi_2 = x, -x$; $\phi_3 = y$; $\phi_4 = x$; $\phi_5 = 2(x), 2(-x)$; $\phi_{rec} = x, 2(-x), x$. The last 90° pulses on $^{13}C'$ and $^{13}C^{\alpha}$ remove the dispersive contribution from the lineshape [32,33].

without prolonging the overall pulse sequence element. Thus, the proposed pulse sequence element combines the advantages of both the iHNCA [12] and intra-HNCA [15] schemes. The coherence transfer function to the proposed pulse sequence element can be given using Eq. (3):

$$\sin(2\pi^1 J_{NC'} T_N)\sin(4\pi^1 J_{NC^\alpha} T_a)\sin(4\pi^2 J_{NC^\alpha} T_a) \times \sin(2\pi^1 J_{C'C^\alpha} T_C)\exp(-2(2T_a - T_C)/T_{2,N}) \times \exp(-2T_C/T_{2,MQ}). \quad (3)$$

It can be realized that when $2(2T_a - T_C) = 2T_N$, the overall length of the pulse sequence is identical to the intra-HNCA element [15,16]. Typically, however, on small and medium sized proteins it is advisable to set the ^{15}N–$^{13}C^\alpha$ transfer delay to ~50 ms in order to optimize transfer to residues in α-helix and to provide the best overall suppression of the sequential cross peaks [12].

The proposed pulse sequence element is versatile and can be utilized as a building block for several experiments to provide solely intraresidual connectivities. Fig. 1D shows the optimized *out and back* type intraresidual iHNCA experiment for correlating $^1H^N(i)$, $^{15}N(i)$, and $^{13}C^\alpha(i)$ chemical shifts. In a manner analogous to the conventional HNCA experiment, the famous HNCACB experiment [8] can be equipped with the proposed intraresidual pulse sequence element. The corresponding intraresidual iHNCACB experiment is illustrated in Fig. 1E. The iHNCACB pulse sequence contains an additional transfer step $2T_{CC}$ during which the desired coherence is transferred from the $^{13}C^\alpha(i)$ nucleus partly to $^{13}C^\beta(i)$ spin prior to the t_1 period.

As it has been suggested [12] and demonstrated [14], the intraresidual transfer scheme with TROSY [22] implementation can be very useful for assigning larger proteins as an alternative to the familiar HN(CO)CA–TROSY experiment [23]. Fig. 2 shows two implementations of TROSY based iHNCA experiments. The *out and back* version of the proposed iHNCA–TROSY scheme is depicted in Fig. 2A. It is basically identical to the iHNCA scheme of Fig. 1D, expect for omitting the proton and nitrogen decoupling fields. In addition, the ^{13}C–^{15}N back-INEPT and the first spin-state-selective filter in the TROSY element are concatenated to reduce the time the ^{15}N spin remains in the transverse plane [19,24].

The out and other way back type iHNCA–TROSY experiment is illustrated in Fig. 2B. It can be very useful for assigning high molecular weight proteins at the highest magnetic field [12,14]. The initial part of the pulse scheme (prior to the t_1 period) is identical to the *out and back* type iHNCA–TROSY experiment (Fig. 2A). However, after labeling the $^{13}C^\alpha$ chemical shift during t_1, the desired coherence is converted directly back to

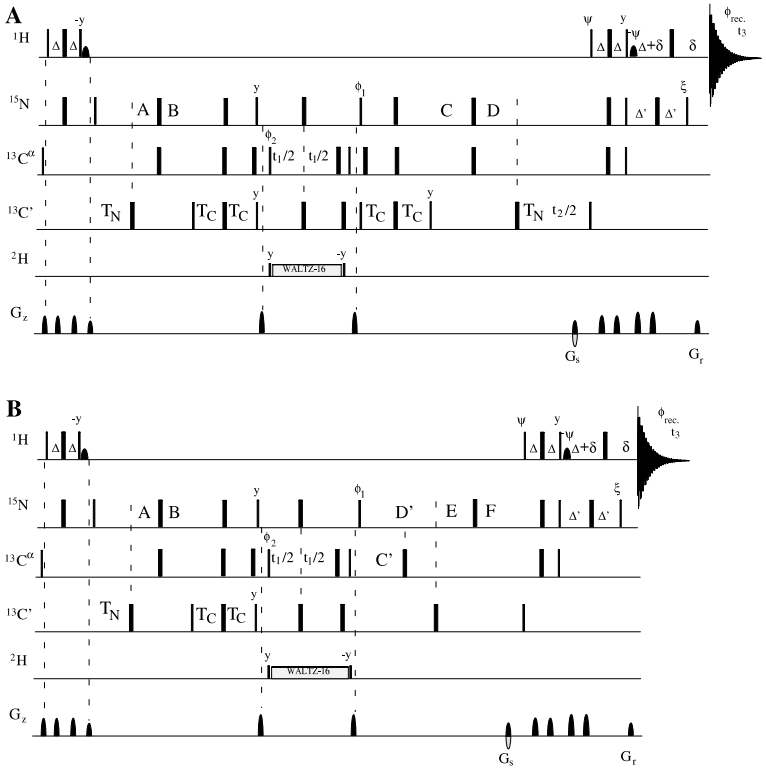

Fig. 2. (A) The streamlined *out and back* type iHNCA–TROSY and (B) *out and other way back* type iHNCA–TROSY experiments for recording solely intraresidual $^{13}C^\alpha(i)$, $^{15}N(i)$, and $^1H^N(i)$ connectivities in $^{13}C/^{15}N/(^2H)$ labeled proteins. All parameters are identical to the pulse sequences in Fig. 1 except for the following delays employed: $C = 2T_a - (T_C + \Delta + t_2/2)$; $D = 2T_a - (T_N + T_C + \Delta)$; $C' = t_2/2 + T'_a$; $D' = T'_N$; $E = (1-\kappa)*t_2/2$; $F = T'_N - \kappa * t_2/2$; $1/(4J_{NC'}) \geqslant T'_N \geqslant T'_a$; $0 \leqslant \kappa \leqslant T'_N/t_{2,max}$. In addition, the quadrature detection in ^{15}N dimension is obtained using the sensitivity-enhanced, gradient selected TROSY scheme [34], i.e., two data sets are collected (I): $\psi = x$, $\xi = y$, (II) $\psi = -x$, $\xi = -y$, with simultaneous change in the gradient G_S polarity. Phase cycling: $\phi_1 = x$ (scheme A); $\phi_1 = y$ (scheme B); $\phi_2 = x, -x$; $\phi_{rec} = x, -x$.

^{15}N single-quantum coherence. Subsequently, the anti-phase $^{1}J_{NC^{\alpha}}$ and $^{1}J_{NC'}$ couplings are refocused and the magnetization is transferred back to the amide proton prior to acquisition [12,14]. In this way, the $^{13}C^{\alpha}$–$^{13}C'$ back-INEPT step can be eliminated, which efficiently reduces by 50% the time the fast relaxing $^{13}C'$ spin remains in the transverse plane in comparison, for instance, to the *out and back* iHNCA–TROSY (Fig. 2A) or HN(CO)CA–TROSY experiments consisting of two $^{13}C^{\alpha}$–$^{13}C'$ INEPT steps. In addition, the ^{15}N–^{13}C back transfer step can be shortened, and is set typically close to 30 ms, to minimize sensitivity losses on larger proteins [5,12,14].

3. Material and methods

The pulse schemes were tested on 1.9 mM uniformly ^{15}N, ^{13}C labeled human ubiquitin (Asla, Riga, Latvia) dissolved in 95/5% H_2O/D_2O, 10 mM potassium phosphate buffer, pH 5.8, in a sealed Wilmad 535 NMR tube at 30 °C, and on 1.0 mM U-^{15}N, ^{13}C, and ^{2}H labeled Cel6a dissolved in 95/5% H_2O/D_2O, 10 mM potassium phosphate buffer, pH 6.0, in a 270 μl Shigemi microcell at 40 °C.

All 3D spectra were acquired on a Varian Unity INOVA 800 MHz spectrometer equipped with a ^{1}H/^{15}N/^{13}C triple-resonance probehead and an actively shielded triple-axis gradient system. The proposed intraresidual HNCA, iHNCA [12], intra-HNCA [15], and the conventional HNCA [1,2] were recorded under identical conditions at 30 °C, using human ubiquitin as the test molecule. The delays used were $2T_a = 25$ ms, $T_N = 16.7$ ms, $T_C = 4.55$ ms, $\Delta = 5.3$ ms, and δ = gradient + field recovery delay. The number of complex points were 64, 64, and 920, corresponding to acquisition times of 12, 25, and 51 ms in ^{13}C, ^{15}N, and ^{1}H dimensions, respectively. Two transients per FID were used, resulting in a total acquisition time of 10.5 h for the each 3D spectrum. The F_2 dimension was extended by forward linear prediction to 128 complex points. The data were zero-filled to $256 \times 256 \times 1024$ points before Fourier transform and shifted squared sine-bell weighting functions were applied in all three dimensions.

The iHNCACB spectrum was acquired on ubiquitin as a 2D $^{13}C^{\alpha}/^{13}C^{\beta}$, $^{1}H^{N}$ correlation experiment ($t_2 = 0$) using four transients per FID with 128, 2048 complex points and the corresponding acquisition times of 10 and 51 ms in t_1 and t_3, respectively. Total acquisition time was 21 min. The data were zero-filled to 1024×2048 points before Fourier transform and shifter squared sine-bell weighting functions were applied to both dimensions.

The 3D iHNCA–TROSY spectrum, acquired with the pulse scheme in Fig. 5B, was recorded on Cel6a using four transients per FID with 64, 32, and 1126 complex points in F_1, F_2, and F_3 dimensions, respectively. This corresponds to acquisition times of 9, 12, and 51 ms in t_1, t_2, and t_3, respectively. Total acquisition time was 10 h. The data were zero-filled to $128 \times 64 \times 1024$ points before Fourier transform and shifted squared sine-bell weighting functions were applied in all three dimensions.

4. Results and discussion

To obtain experimental verification of the performance of the proposed intraresidual pulse scheme, the optimized *out and back* style iHNCA pulse scheme was compared to the *out and back* iHNCA [12] and intra-HNCA [15] experiments. Fig. 3 represents spectra recorded on human ubiquitin, a small 8.6 kDa (76 amino acid residues) protein consisting of five β-strands, one 12-residue α-helix, and two 3_{10}-helices [25]. The overlaid traces from the proposed iHNCA (solid line) and intra-HNCA (dashed line) clearly demonstrate the gain in sensitivity, especially for the α-helical residues. In addition,

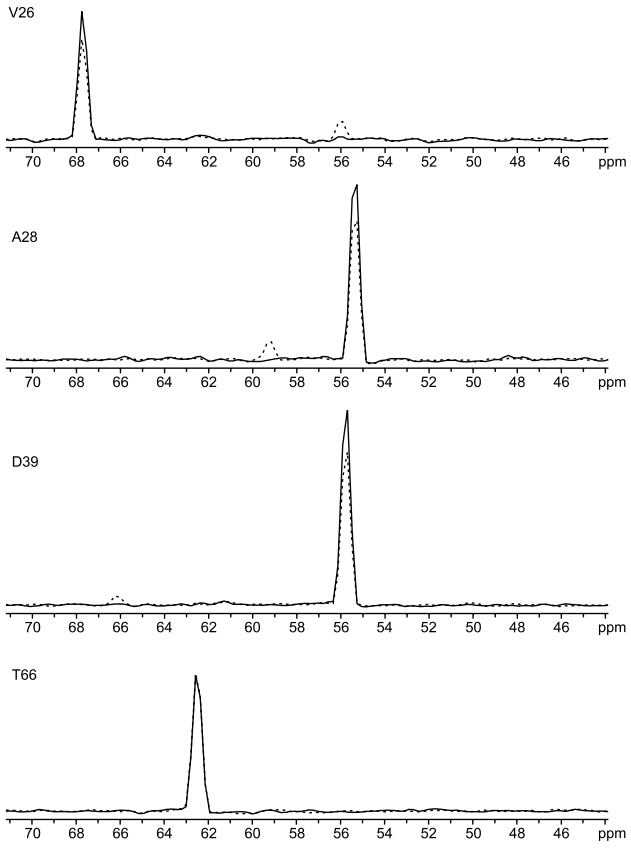

Fig. 3. Four representative F_1 slices from the two 3D intraresidual HNCA spectra measured from human ubiquitin. Data from intra-HNCA [15] are represented with dashed lines, and data from the optimized iHNCA experiment with solid lines. Residues Val26 and Ala28 are found in the α-helical region of ubiquitin structure whereas Asp39 is located in a short 3_{10}-helix, and Thr66 in a β-strand.

the level of suppression for the undesired sequential pathway is higher for the proposed experiment, as can be readily observed for the helical residues, Val26, Ala28, and Asp39.

To estimate the coherence transfer efficiency for the intraresidual pathway in the optimized experiment, the relative peak intensities as a function of ubiquitin's amino acid sequence in the restructured iHNCA and intra-HNCA spectra were examined (Fig. 4A). As can be easily recognized, the coherence transfer efficiency in the proposed experiment is significantly better (ca. 12–23%) for the residues located in the α-helix (residues 23–34) and in the short 3_{10}-helices (residues 38–40 and 57–59). More importantly, as the theoretical coherence transfer efficiency in the intraresidual experiments is generally weaker for residues in helical substructures than for residues located in β-strands, the proposed pulse scheme especially improves the sensitivity of those residues that are limiting the assignment procedure due to their lower experimental sensitivity. The coherence transfer for helical residues was modestly better in iHNCA [12] compared to intra-HNCA [15] due to the longer transfer delay ($4T_a$) used, but not as efficient as the proposed

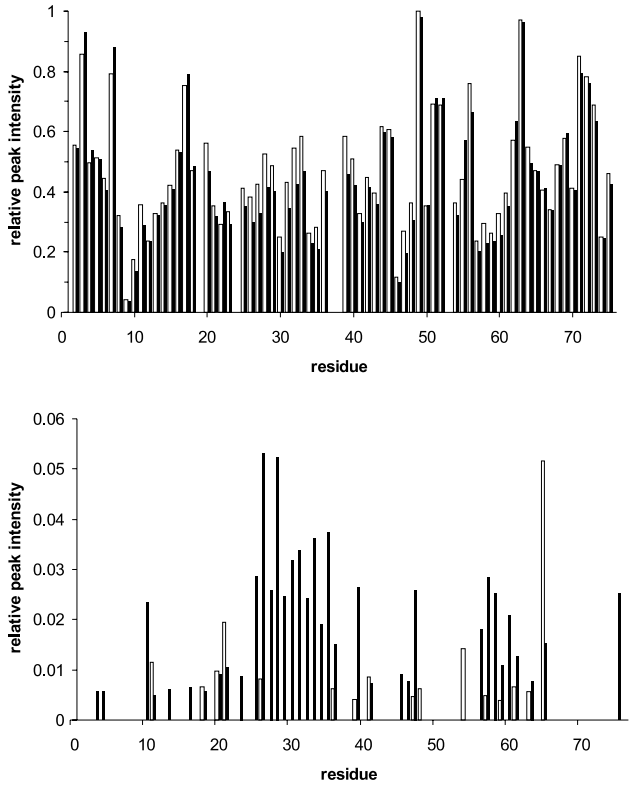

Fig. 4. Comparison of relative peak intensities in the two intraresidual HNCA spectra. (A) Relative intensities of the intraresidual peaks, with white bars representing peaks from the iHNCA experiment with the optimized intraresidual transfer scheme and black bars from intra-HNCA [15]. The height of the bar represents the intensity relative to the most intense peak of the two spectra, Gln49. (B) Relative intensities of the sequential peaks.

pulse scheme (data not shown). As is assumed based on theoretical calculations, the succeeding $4T_a$ and $2T_C$ transfer delays used in the iHNCA scheme [12] compromise the sensitivity in comparison to the new experiment and partly also to intra-HNCA. This is because in iHNCA ^{15}N and $^{13}C'$ spins are susceptible to transverse relaxation for a longer period than in the optimized intraresidual pulse sequence element.

The intensity of the proposed iHNCA experiment was found to be equal or superior to the conventional HNCA [1,2] for the residues in the β-strands aside from a few exceptions. As expected, the coherence transfer for the helical residues was not as efficient as in the conventional HNCA experiment, although in the new scheme the advantages of the original intraresidual schemes [12,15] were merged and consequently the coherence transfer for the residues in helices was significantly improved. However, on larger proteins with ^{15}N transverse relaxation times significantly shorter than ca. 90 ms, the sensitivity of the intraresidual experiments will be greatly diminished in comparison to the conventional HNCA experiment [5].

It is also of interest to inspect the intensity of the undesired sequential cross peaks. Fig. 4B confirms the theoretical presumptions that the amount of leakage of the sequential correlation in the intraresidual spectrum is usually observed for helical residues if the $^1J_{NC^\alpha} + {}^2J_{NC^\alpha}$ transfer delay is significantly shorter than ~50 ms [12]. In the proposed scheme, the transfer delay was set to 50 ms, and consequently a clearly better suppression of sequential peaks was obtained for the residues in helices. In general, the suppression was significantly better or of equal quality for the optimized pulse scheme. It is noteworthy that the sequential peaks with relative intensity below the level of ~0.01 in Fig. 4B are basically at the noise-level. However, the most intensive sequential correlations in ubiquitin (e.g., Asn25) exhibit a higher intensity than the weakest intraresidual cross peak (Thr9).

Fig. 5 represents the iHNCACB spectrum, recorded as a 2D ^{13}C, $^1H^N$ correlation experiment ($t_2 = 0$) from ubiquitin. Only intraresidual $^{13}C^\alpha$ and $^{13}C^\beta$ resonances are observed for each $^1H^N$ frequency, which greatly facilitates the manual or automatic sequential assignment in the case of poorly dispersed aliphatic carbon shifts.

Fig. 6 illustrates a demonstrative 2D excerpt from the 3D iHNCA–TROSY spectrum, recorded using the *out and other way back* iHNCA scheme equipped with the proposed intraresidual transfer element (Fig. 2B). The spectrum was recorded from a 30.4 kDa (286 amino acid residues), uniformly ^{15}N, ^{13}C, and ^2H labeled protein Cel6A from the thermophilic soil bacterium *Thermobifida fusca* [26] at 800 ^1H MHz at 40 °C in 10 h. As can be seen, solely intraresidual cross peaks are observed for each residue. The sensitivity of the streamlined iHNCA experiment was found to be superior to the original

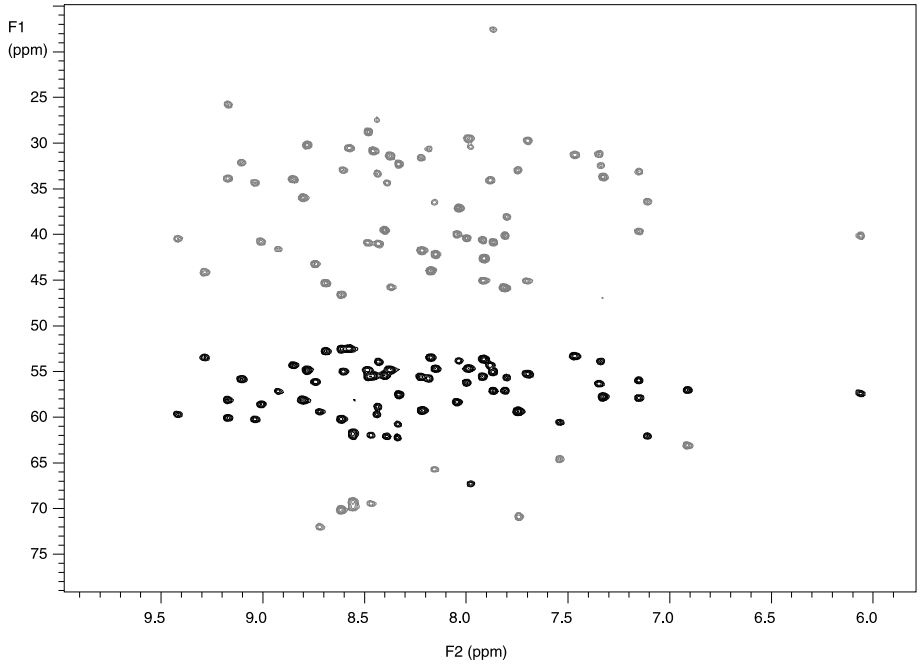

Fig. 5. Enlargement from the $^{13}C^{\alpha}/^{13}C^{\beta}$ region of the iHNCACB spectrum, recorded with the pulse scheme depicted in Fig. 1E. The spectrum shows solely intraresidual $^{13}C^{\alpha/\beta}(i)$, $^{1}H^{N}(i)$ cross peaks. $^{13}C^{\beta}$ resonances, displayed with gray contours, are in the opposite phase with respect to $^{13}C^{\alpha}$ signals. The quality of suppression for the sequential pathway is similar to the iHNCA experiment.

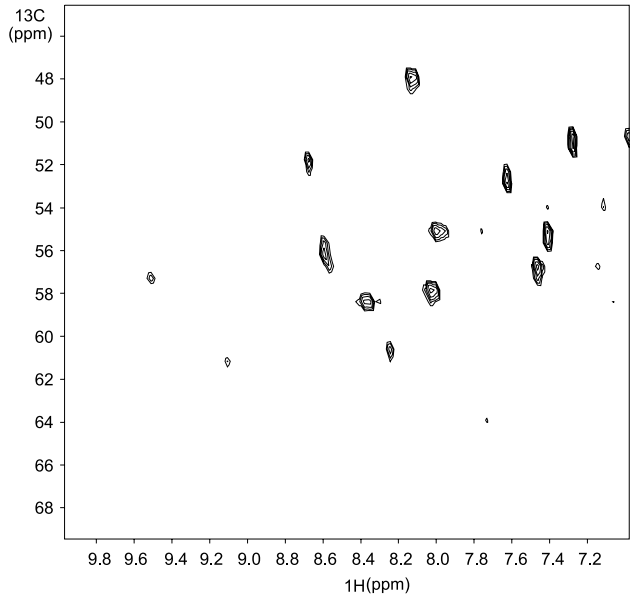

Fig. 6. 2D $^{13}C^{\alpha}$, $^{1}H^{N}$ planes extracted from the 2D iHNCA–TROSY spectrum of a 30.4 kDa, uniformly $^{15}N/^{13}C/^{2}H$ labeled protein Cel6A. The data were recorded using the *out and other way back* type iHNCA–TROSY scheme depicted in Fig. 2B. Note that the weakest correlations do not have their intensity maximum in the extracted plane.

scheme [12,14] for Cel6a at the elevated temperature of 40 °C (data not shown). This holds the promise for further extending the feasibility of the intraresidual experiments for the assignment of larger proteins.

5. Conclusions

We have introduced the optimized intraresidual pulse sequence element and demonstrated its feasibility on two proteins. The proposed intraresidual pathway selection scheme provides improved sensitivity for the new type of triple-resonance experiments, which utilize the so-called intraresidual transfer in order to establish solely intraresidual connectivities in ^{15}N, ^{13}C, ^{2}H labeled proteins. The optimized intraresidual transfer element enables unrestricted adjustment of individual transfer delays without unnecessary lengthening of the pulse sequence. It is then possible to set the transfer delays in accordance with the relaxation properties of ^{15}N and $^{13}C'$ spins. For example, at the highest magnetic field, the $^{13}C'$–$^{13}C^{\alpha}$ transfer delay can be shortened without affecting the ^{15}N–^{13}C transfer. The intraresidual experiments are complementary with the familiar HN(CO)CA based experiments which display only sequential connectivities for each amide spin pair. The intraresidual experiments can then be used concomitantly with sequential experiments to provide minimum resonance overlap for the efficient sequential assignment. On the other hand, the *out and other way back* type intraresidual experiments can also be used together with HNCA (or HNCACB) experiments for instance at the highest magnetic field, where rapid transverse relaxation of the carbonyl carbon nucleus seriously reduces the sensitivity of the HN(CO)CA scheme.

Acknowledgment

This work was financially supported by the Academy of Finland.

References

[1] L.E. Kay, M. Ikura, R. Tschudin, A. Bax, 3-dimensional triple-resonance NMR-spectroscopy of isotopically enriched proteins, J. Magn. Reson. 89 (1990) 496–514.
[2] A. Bax, M. Ikura, An efficient three-dimensional NMR technique for correlating the proton and nitrogen backbone amide resonances with the alpha carbon of the preceding residue in uniformly 13C/15N enriched proteins, J. Biomol. NMR 1 (1991) 99–104.
[3] A. Bax, S. Grzesiek, Methodological advances in protein NMR, Acc. Chem. Res. 26 (1993) 131–138.
[4] M. Sattler, J. Schleucher, C. Griesinger, Heteronuclear multidimensional NMR experiments for the structure determination of proteins in solution employing pulsed field gradients, Prog. Nuc. Magn. Reson. Spectr. 34 (1999) 93–158.
[5] P. Permi, A. Annila, Coherence transfer in proteins, Prog. Nucl. Magn. Res. Spectr. 44 (2004) 97–137.
[6] S. Grzesiek, A. Bax, An efficient experiment for sequential backbone assignment of medium-sized isotopically enriched proteins, J. Magn. Reson. 99 (1992) 201–207.
[7] S. Grzesiek, A. Bax, Correlating backbone amide and side-chain resonances in larger proteins by multiple relayed triple resonance NMR, J. Am. Chem. Soc. 114 (1992) 6291–6293.
[8] M. Wittekind, L. Mueller, HNCACB, a high-sensitivity 3D NMR experiment to correlate amide-proton and nitrogen resonances with the alpha-carbon and beta-carbon resonances in proteins, J. Magn. Res. 101B (1993) 201–205.
[9] T. Yamazaki, W. Lee, M. Revington, D.L. Mattiello, F.W. Dahlquist, C.H. Arrowsmith, L.E. Kay, An HNCA pulse scheme for the backbone assignment of N-15, C-13, H-2 -labeled proteins—application to a 37-kDa Trp repressor DNA complex, J. Am. Chem. Soc. 116 (1994) 6464–6465.
[10] X. Shan, K.H. Gardner, D.R. Muhandiram, N.S. Rao, C.H. Arrowsmith, L.E. Kay, Assignment of N-15, C-13(alpha), C-13(beta), and HN resonances in an N-15, C-13, H-2 labeled 64 kDa trp repressor-operator complex using triple-resonance NMR spectroscopy and H-2-decoupling, J. Am. Chem. Soc. 118 (1996) 6570–6579.
[11] D.S. Wishart, B.D. Sykes, The C-13 chemical-shift index—a simple method for the identification of protein secondary structure using C-13 chemical-shift data, J. Biomol. NMR 4 (1994) 171–175.
[12] P. Permi, Intraresidual HNCA: an experiment for correlating only intraresidual backbone resonances, J. Biomol. NMR 23 (2002) 201–209.
[13] K. Ding, A.M. Gronenborn, Novel 2D triple-resonance NMR experiments for sequential resonance assignments of proteins, J. Magn. Reson. 156 (2002) 262–268.
[14] D. Nietlispach, Y. Ito, E.D. Laue, A novel approach for the sequential backbone assignment of larger proteins: selective intra-HNCA and DQ-HNCA, J. Am. Chem. Soc. 124 (2002) 11199–11207.
[15] B. Brutscher, Intraresidue HNCA and COHNCA experiments for protein backbone resonance assignment, J. Magn. Reson. 156 (2002) 155–159.
[16] B. Bersch, E. Rossy, J. Coves, B. Brutscher, Optimized set of two-dimensional experiments for fast sequential assignment, secondary structure determination, and backbone fold validation of C-13/N-15-labelled proteins, J. Biomol. NMR 27 (2003) 57–67.
[17] F. Delaglio, D.A. Torchia, A. Bax, Measurement of nitrogen-15 carbon-13 J couplings in Staphylococcal nuclease, J. Biomol. NMR 1 (1991) 439–446.
[18] J. Wirmer, H. Schwalbe, Angular dependence of (1)J(N-i,C-alpha i) and (2)J(N-i,C alpha(i-1)) coupling constants measured in J-modulated HSQCs, J. Biomol. NMR 23 (2002) 47–55.
[19] J.P. Loria, M. Rance, A.G. Palmer, III, Transverse-relaxation-optimized (TROSY) gradient-enhanced triple-resonance NMR spectroscopy, J. Magn. Reson. 141 (1999) 180–184.
[20] P. Permi, A. Annila, A new approach for obtaining sequential assignment of large proteins, J. Biomol. NMR 20 (2001) 127–133.
[21] P. Permi, A. Annila, Evaluation and optimization of coherence transfer in high molecular weight systems, J. Magn. Reson. 155 (2002) 123–130.
[22] K. Pervushin, R. Riek, G. Wider, K. Wüthrich, Attenuated T-2 relaxation by mutual cancellation of dipole–dipole coupling and chemical shift anisotropy indicates an avenue to NMR structures of very large biological macromolecules in solution, Proc. Natl. Acad. Sci. USA 94 (1997) 12366–12371.
[23] M. Salzmann, G. Wider, K. Pervushin, H. Senn, K. Wüthrich, TROSY-type triple-resonance experiments for sequential NMR assignments of large proteins, J. Am. Chem. Soc. 121 (1999) 844–848.
[24] M. Salzmann, G. Wider, K. Pervushin, K. Wüthrich, [C-13]-constant-time [N-15,H-1]-TROSY–HNCA for sequential assignments of large proteins, J. Biomol. NMR 15 (1999) 181–184.
[25] G. Cornilescu, J.L. Marquardt, M. Ottiger, A. Bax, Validation of protein structure from anisotropic carbonyl chemical shifts in a dilute liquid crystalline phase, J. Am. Chem. Soc. 120 (1998) 6836–6837.
[26] M. Spezio, D.B. Wilson, P.A. Karplus, Crystal-structure of the catalytic domain of a thermophilic endocellulase, Biochemistry 32 (1993) 9906–9916.
[27] S. Grzesiek, A. Bax, The importance of not saturating H2O in protein NMR—application to sensitivity enhancement and NOE measurements, J. Am. Chem. Soc. 115 (1993) 12593–12594.
[28] L.E. Kay, P. Keifer, T. Saarinen, Pure absorption gradient enhanced heteronuclear single quantum correlation spectroscopy with improved sensitivity, J. Am. Chem. Soc. 114 (1992) 10663–10665.
[29] J. Schleucher, M. Sattler, C. Griesinger, Coherence selection by gradients without signal attenuation—application to the 3-dimensional HNCO experiment, Angew. Chem. Int. Ed. Engl. 32 (1993) 1489–1491.
[30] D. Marion, M. Ikura, R. Tschudin, A. Bax, Rapid recording of 2D NMR-spectra without phase cycling—application to the study of hydrogen-exchange in proteins, J. Magn. Reson. 85 (1989) 393–399.
[31] A.J. Shaka, J. Keeler, T. Frenkiel, R. Freeman, An improved sequence for broxad-band decoupling—Waltz-16, J. Magn. Reson. 52 (1983) 335–338.
[32] P. Permi, T. Sorsa, I. Kilpeläinen, A. Annila, HN(alpha/beta-COCA-J) experiment for measurement of (1)J(C′C alpha) couplings from two-dimensional [N-15, H-1] correlation spectrum, J. Magn. Reson. 141 (1999) 44–51.
[33] D. Yang, L.E. Kay, Improved lineshape and sensitivity in the HNCO-family of triple resonance experiments, J. Biomol. NMR 14 (1999) 273–276.
[34] J. Weigelt, Single scan, sensitivity- and gradient-enhanced TROSY for multidimensional NMR experiments, J. Am. Chem. Soc. 120 (1998) 10778–10779.